Additive Spatially Correlated Noise Suppression by Robust Block Matching and Adaptive 3D Filtering

Oleksii Rubel and Vladimir Lukin

National Aerospace University "KhAI," Department of Information and Communication Technologies, Kharkiv, Ukraine
E-mail: o.rubel@khai.edu

Karen Egiazarian

Tampere University of Technology, Signal Processing Laboratory, Tampere, Finland

Abstract. *The evolution of modern sensors for image acquisition brings as much obstacles as many possibilities to obtain multidimensional data with high resolution and rich information. One of the most perceptible destructive factors in visual data is noise. Due to complexity of modern sensors and approaches to signal collecting or preprocessing, noise model becomes complicated. The article's goal is to introduce and solve a problem of suppressing additive spatially correlated noise (ASCN) which is present in images due to different sources and has various levels of correlation. It is shown that even modern filters attempting to suppress correlated noise often demonstrate unsatisfactory efficiency. Here we propose and analyze two modifications of 2D discrete cosine transform (DCT) based filter and the state-of-the-art BM3D technique. Both are based on accounting spatial spectrum of the noise by setting frequency-dependent thresholds. Furthermore, the modified BM3D filter exploits a similarity measure robust to noise spectrum in block matching.* © 2018 Society for Imaging Science and Technology.
[DOI: 10.2352/J.ImagingSci.Technol.2018.62.6.060401]

1. INTRODUCTION

A large amount of available information about real-world objects obtained from modern imaging systems is provided by complex sensors and appropriate preprocessing of obtained data to represent images in a convenient form [1]. Images (multidimensional data) with high resolution can be a rich source of useful information for various applications [2, 3]. Sophisticated methods of signal collecting and operations applied to acquired data bring informative features but, at the same time, introduce distortions. One of dominant destructive factors in visual data is noise [4] that can originate from various sources and have different nature. In practice, the so-called denoising procedure is applied to improve the quality of images.

Basically, the denoising takes into account the type of noise, its model and parameters. The commonly accepted noise model in image processing is an additive white Gaussian noise [4]. Practically, this assumption is quite idealistic because the noise distribution can be other than Gaussian and power spectrum can be nonuniform [5]. Such disaccord can affect negatively the efficiency of image

denoising or postprocessing and, consequently, visual quality of output image [6]. Thus one has to use more adequate noise models and adapt image processing to them. Spatially correlated noise (SCN) in images arises in general from mutual impact of neighbor signal samples and its noisy parts having the same characteristics. Due to this, SCN power spectrum concentrates mostly in low spatial frequencies [7]. As a result, its appearance on images has a "grain"-like structure. The size of such "grains" depends on spatial correlation degree, i.e., the area of neighbor noisy signal samples impacting the noise component in each pixel. There are many observed variants of SCN: additive, signal dependent and mixed. In this article, we consider only the case of additive spatially correlated noise (ASCN) suppression. For other models of SCN, reduction to additive model (ASCN) can be performed (for example, by applying a proper variance stabilizing transform [8]).

Let us consider in detail different origins of SCN and its characteristics in spatial and spectral domains. The first origin of spatially correlated noise is speckle noise in synthetic-aperture radar systems [8] in remote sensing. SAR-based imagery acquires data in the following way. A set of sensors mounted on a moving platform collects signals scattered from a sensed surface. While the platform is moving, a way the sensor travels over a target creates a large-sized antenna aperture to obtain the signal with higher resolution. Multiple signal reflections taken from the same target on a surface collected in different moments of time have random structure. The SCN origin in this case deals with principles of signal collecting and spatial sampling.

Other sources of spatially correlated noise presence are caused by data preprocessing. One of them is a joint processing of two or more satellite images of the same area in different moments of time or by various sensors [9]. Nonlinear operations with data result in changing the statistical and spectral properties of the noise. Spatially correlated noise can be also caused by demosaicing applied to raw data in digital cameras [10]. The sensors with Bayer filter mosaic produce raw data that are demosaiced (interpolated). Any interpolation uses sensor pixels depending on wavelength illumination with close location. While signal processing exploiting neighbor samples of the same color is performed, spatial correlation of the resulting noise appears.

The latter noise origins deal with software processing of already acquired data. In such circumstances, the standard noise model is no longer adequate and special efforts to denoising adapting to noise properties shall be made. Note that researchers arrive at the necessity of using SCN models in applications of image processing [11] such as magnetic resonance imaging, thermals and cameras.

There are plenty of modern denoising techniques oriented on AWGN suppression [12]. It is worth mentioning the state-of-the-art filters [13] for AWGN case that have high efficiency. There are filters performing in spatial domains like Nonlocal means [14] (NLM) that uses similarity of image patches in a certain region and carries out denoising by the joint processing of the collected similar parts of noisy signals. Due to patch similarity of the signal component, filtering efficiency greater than that for classical window-based denoising methods is achievable. Spatially iterative filtering SAIF [15] has been proposed as a further evolution of NLM exploiting its kernel and performing optimization for its parameters. One exemplar of an effective technique that works only with extracted features in spatial domain is principal component analysis with local pixel grouping [16] (LPG-PCA). Note that the filters with data processing in spectral domain usually demonstrate higher performance than spatial-domain filters. The basic principle of such denoising is to represent the signal in a sparse form and to distinguish it from noise distributed over the full dataset. Bayesian least squares of Gaussian scale mixtures (BLS-GSM) [17] and 2D DCT-based filter (DCTF) [18] exploit the spectral representation of signal and remove the noise by a shrinkage. Using both approaches of nonlocal denoising and data processing in spectral domain, the block matching and 3D filtering technique (BM3D) [19] outperforms the aforementioned filters in many cases, especially in images with a high degree of self-similarity. Finally, among other classes of filters, it is worth mentioning the idea of a global nonlocal approach to restore image patches from previously learned dictionaries under image data. The K-SVD [20] and K-LLD [21] techniques form their dictionaries in different ways: globally from entire images and locally from some dataset.

As we have stated above, there are two modern principles that allow to suppress noise effectively—the nonlocal approach, i.e., block matching to collect together similar image patches, and sparse representations of signal to distinguish it from the noise easily. These approaches, in standard usage, are not adapted to SCN. There are several known attempts to adapt block matching for SCN [22] and denoising in spectral domain [23] applied to SAR images. These modifications have been proposed for certain models of SCN with multiplicative nature of speckle. There is also one method that employs modeling the signal of interest in the wavelet domain to attenuate ASCN [24]. However, such modifications are unitary and oriented on particular SCN cases with certain spatial correlation degree. In this article, we propose the modifications of two existing denoising techniques oriented on ASCN suppression with
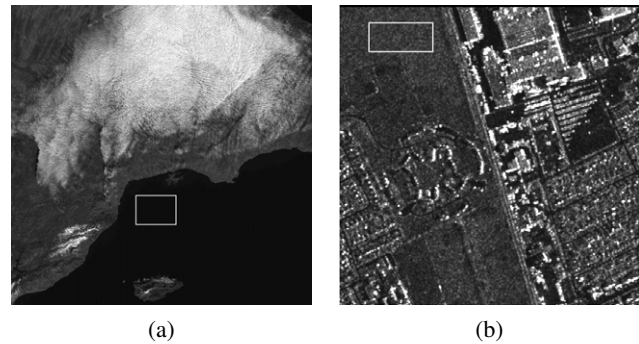
Figure 1. Real-life images corrupted by spatially correlated noise: (a) the JPEG 2000-compressed image provided by Sentinel-2A system and (b) one polarization image obtained from TerraSAR-X sensor.

different correlation degrees. Note that for multiplicative or signal-dependent SCN suppression the homomorphic processing and/or variance stabilizing can be applied [25].

The article is organized as follows. Section 2 shows two real-life cases of SCN with estimated noise spectrum characteristics. The modeling method of ASCN having a variable spatial correlation degree is also presented. Section 3 deals with efficiency analysis for modern denoising techniques applied to different ASCN cases. Section 4 describes adaptation of two filters: DCTF and BM3D. Finally, Section 5 presents denoising results with outcomes and examples.

2. REAL-WORLD SPATIALLY CORRELATED NOISE AND ITS MODELING

Let us consider real-life cases of spatially correlated noise. The first one is a satellite image obtained from Sentinel-2A compressed by JPEG 2000 and corrupted by ASCN with a low correlation degree (Figure 1(a)). A more detailed information about this image can be found using its entity id—L1C_T35TNF_A008441_ 20170202T090155. Detailed analysis of noise parameters can be found in article [26]. The second one is a single polarization image produced by TerraSAR-X system. The noise model in this case is speckle, the signal-dependent SCN with a high degree of spatial correlation that can be observed from Fig. 1(b).

Most denoising techniques that perform in a spectral domain usually have a block size of 8x8 pixels and SCN can be characterized by normalized power spectrum in block-wise manner [27]. Practically any image has homogeneous regions (also treated as noninformative). Such regions can be chosen manually. Thus, it is possible to assume that only pure noise is observed and estimation of its parameters can be done. After homogeneous regions have been extracted from an image, the obtained dataset can be divided into nonoverlapping blocks. In Fig. 1, examples of such regions are marked by white rectangles. Every block is then transformed by DCT and transform coefficients are squared to obtain energy of the noise for each frequency component. The first component (DC) is not taken into account since it corresponds to mean level of the signal that is out of our interest. After all energy values of each component for all transformed blocks are
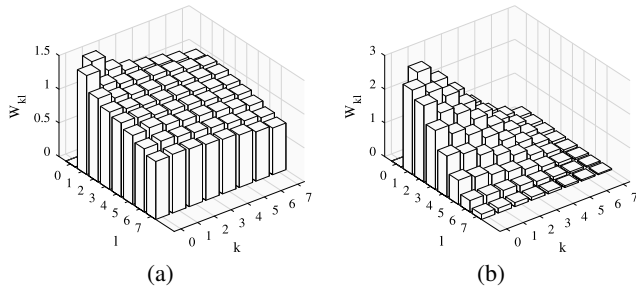
Figure 2. Block-wised (8x8 pixels) normalized noise spectrum in DCT domain for (a) Sentinel product image and (b) TerraSAR-X image. Noise spectrum for both cases has been calculated in homogeneous image regions divided into blocks (marked by white rectangles in Fig. 1) without signal components.

Figure 3. (a) The target function for SCN modeling ($\sigma_G = 1$) and (b) block-wised normalized noise spectrum in DCT domain for generated SCN case.

averaged, the normalized noise block spectrum is obtained in the following manner:

$$W_{kl} = \sqrt{\frac{\overline{B_{kl}^2} \cdot (b^2 - 1)}{\sum_{k,l} \overline{B_{kl}^2}}}, \qquad (1)$$

where B is a transformed block in the homogeneous region, b is a block side, k and l are indices of components in the transformed block, and W is a normalized spectrum. See examples of calculated normalized block spectrum from real-life images in Figure 2.

Note that the shown normalized spectra differ from each other. The main part of energy unlike the case of AWGN (with uniform distribution of all frequency components) is concentrated mostly at low frequencies. The presented examples demonstrate that spatially correlated noise can have different degrees of spatial correlation. The case of SCN with a minimal spatial correlation degree practically has no difference with respect to AWGN case when the normalized block spectrum has all weights equal to 1. In case of SCN with a high degree of correlation, the normalized spectrum values can differ by one or even two orders.

The next question arises—how spatially correlated noise can be modeled to generate noisy images that have noise characteristics corresponding to a considered practical application? Due to the low-frequency nature of SCN, it is possible to model it in the reverse order. The spectrum of AWGN realization can be modified via low-pass filtering and transformed back into the spatial domain. A modification of a spatial Fourier spectrum by a target function will produce a desired degree of spatial correlation. A 2D Gaussian function that amplifies low frequencies and reduces high frequencies is one of the examples of such target function:

$$G_{ij} = \exp\left[-\pi * \frac{(i^2 + j^2)}{2 * \sigma_G^2}\right], \qquad (2)$$

where σ_G is a "tuning" parameter for varying the degree of spatial correlation, i and j are target function indices, and G is a target function. After modification of the Fourier spectrum of AWGN realization by the target function (Eq. (2)), the
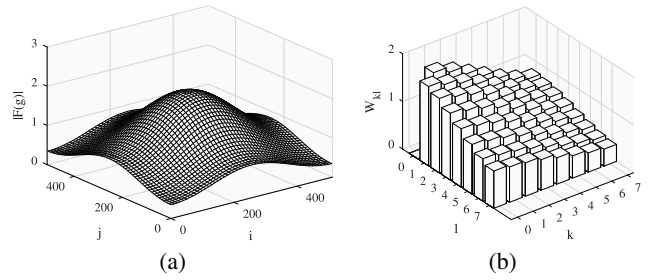
inverse Fourier transform is applied to the pointwise product of the Fourier spectra:

$$N_{SC} = F^{-1}[F(N_{Gaussian}) * F(G)], \qquad (3)$$

where F denotes Fourier transform and N_{SC} is the output SCN realization. After inverse transform, the SCN realization must be corrected by scaling to provide a desired standard deviation of SCN. In Figure 3(a), the example of target function G is shown ($\sigma_G = 1$), the corresponding normalized block DCT spectrum of the noise is presented in Fig. 3(b). The previously shown block normalized spectra for real-life images (Fig. 2) approximately correspond to the modeled cases of SCN with $\sigma_G = 0.8$ and $\sigma_G = 1.5$, respectively. It is possible to assume that AWGN case is observed at $\sigma_G \leq 0.5$.

3. DENOISING EFFICIENCY ANALYSIS FOR FILTERS NOT ADAPTED TO SCN

Now let us consider different cases of ASCN with respect to its spatial correlation degree and assess denoising efficiency for filters intended to remove AWGN. For further analysis, the following filters have been chosen: NLM [14], SAIF [15], LPG-PCA [16], DCTF [18] (2D DCT-based filter), BM3D [19], K-SVD [20] and K-LLD [21]. The used image/noise model for the considered case of additive spatially correlated noise is the following:

$$I_{ij}^n = I_{ij}^{tr} + N_{SC_{ij}}, \qquad (4)$$

where I_{ij}^n are noisy image samples, I_{ij}^{tr} are samples of true image. To obtain more reliable results of denoising, a wide class of test images having different properties should be used. For this purpose, known test images and images from several databases have been used: six images from TID2013 database [28] (#1, 3, 5, 7, 13, 23), the test image "Grass," one texture image from the database USC-SIPI [29] (#7) and two remote sensing test images called "fr01" and "fr02" [30]. In our previous works [31–33], we have considered imaging with different content to understand how image content influences denoising efficiency. It has been demonstrated that the task to suppress noise in texture images is the most difficult, especially if the noise is spatially correlated. Also potential limits of peak signal-to-noise ratio (PSNR) determined in two ways—by nonlocal approach [34] and by the technique [35]—show that various filters demonstrate

Table I. PSNR results and PSNR improvements of denoising applied to images corrupted by ASCN ($\sigma_G = 0.8$) with $SD = 10$.

	TID2013 #1	TID2013 #3	TID2013 #5	TID2013 #7	TID2013 #13	TID2013 #23	Grass	USC-SIPI #7	FR Test #1	FR Test #2
Noisy AWGN	28.145	28.144	28.147	28.144	28.149	28.147	28.236	28.161	28.190	28.153
BM3D AWGN	3.141	8.883	4.339	7.773	1.889	8.787	0.454	3.916	4.098	3.971
Noisy	28.127	28.127	28.130	28.127	28.130	28.128	28.213	28.137	28.171	28.128
DCTF	2.688	7.457	3.212	6.291	1.580	7.653	0.202	2.603	2.954	2.860
BM3D	2.727	8.128	3.810	6.999	1.592	7.922	0.249	3.203	3.626	3.458
NLM	1.257	7.631	2.464	6.312	−1.108	7.421	−5.393	2.425	1.875	1.490
SAIF	2.852	8.045	3.794	6.476	1.864	7.870	0.472	2.945	3.864	3.762
LPG-PCA	−1.063	5.613	0.035	3.669	−2.450	5.973	−3.558	−0.079	−0.152	−0.484
K-SVD	2.815	8.089	3.456	6.707	1.734	7.928	0.229	2.776	3.231	3.141
K-LLD	2.049	6.575	3.239	5.949	1.168	7.074	0.307	2.551	2.983	2.809

Table II. MSSSIM results and MSSSIM improvements for denoising applied to images corrupted by ASCN ($\sigma_G = 0.8$) with $SD = 10$

	TID2013 #1	TID2013 #3	TID2013 #5	TID2013 #7	TID2013 #13	TID2013 #23	Grass	USC-SIPI #7	FR Test #1	FR Test #2
Noisy AWGN	0.961	0.901	0.975	0.948	0.968	0.912	0.994	0.984	0.969	0.966
BM3D AWGN	0.013	0.082	0.013	0.040	0.001	0.072	1e-4	0.005	0.016	0.019
Noisy	0.951	0.878	0.970	0.937	0.959	0.893	0.992	0.980	0.963	0.959
DCTF	0.019	0.095	0.014	0.045	0.006	0.084	1.7e-4	0.004	0.018	0.022
BM3D	0.019	0.099	0.016	0.047	0.005	0.085	1.3e-4	0.005	0.019	0.023
NLM	0.003	0.097	0.010	0.043	−0.022	0.085	−0.016	0.002	0.011	0.015
SAIF	0.019	0.099	0.015	0.045	0.007	0.087	4.5e-4	0.005	0.020	0.024
LPG-PCA	−0.030	0.092	−0.003	0.034	−0.058	0.081	−0.008	−0.015	−0.001	0.003
K-SVD	0.020	0.100	0.014	0.047	0.007	0.088	2e-4	0.005	0.019	0.023
K-LLD	0.013	0.079	0.013	0.039	0.002	0.073	1.5e-4	0.004	0.017	0.020

similar low efficiency. Among the chosen test images, there are highly textured ones—TID2013 #13, Grass, USC-SIPI #7. Other images have, at least, rich texture regions except the images TID2013 #3 and #23.

To assess denoising efficiency, the following metrics of visual quality are used in our analysis—output PSNR, PSNR-HVS-M [36], MSSSIM [37] and FSIM [38]. To characterize the denoising impact, we have also used a metric "improvement" value—the difference between the metric value for the filtered image and the noisy one. Further the prefix "I" before any metric denotes the improvement of denoising.

The testing results are analyzed below for two cases of spatial correlation degree of ASCN mentioned above −$\sigma_G = 0.8$ and $\sigma_G = 1.5$. We call these cases as moderate and large degree of SCN. The ASCN for both degrees are generated with the noise standard deviations equal to 10 and 15, respectively. Moderate ASCN usually takes place after data software processing like demosaicing. On the contrary, the large degree of SCN corresponds to remote sensing images where noise has high intensity. In Tables I

and II, PNSR and MSSSIM results for $SD = 10$ and moderate variant of ASCN are presented. The first two rows of Tables I–VIII data are metrics values for AWGN denoising results. The other data rows correspond to ASCN. Both metric values for noisy images corrupted by AWGN and ASCN are given to analyze visual quality decreasing. Improvements given by the considered filters are shown below. Since the standard BM3D filter is the state-of-the-art technique intended to AWGN removal, its denoising efficiency of AWGN suppression is used to assess improvement of visual quality provided by considered filters.

From data in Table I, it is seen that for images TID2013 #3, 7, 23 that have a quite simple structure and strong self-similarity (further these three images will be called as "simple" in the sense of denoising ease), all filters, especially the nonlocal ones, demonstrate high IPSNR up to 8 dB. It should be stressed that BM3D, NLM, SAIF and K-LLD practically have the best results among all considered filters for such images. The worst results under even moderate ASCN are shown by LPG-PCA. The aforementioned highly textural images are filtered

Table III. PSNR-HVS-M results and PSNR-HVS-M improvements of denoising applied to images corrupted by ASCN ($\sigma_G = 1$) with $SD = 10$.

	TID2013 #1	TID2013 #3	TID2013 #5	TID2013 #7	TID2013 #13	TID2013 #23	Grass	USC-SIPI #7	FR Test #1	FR Test #2
Noisy AWGN	32.201	30.723	32.939	31.615	32.559	30.870	36.425	33.920	32.619	32.628
BM3D AWGN	1.344	6.367	2.074	4.830	0.385	5.838	−0.158	0.521	1.731	2.049
Noisy	27.756	26.901	28.240	27.414	27.969	26.976	30.516	28.701	28.090	28.045
DCTF	1.832	4.464	1.491	3.337	1.099	4.278	0.067	0.475	1.685	1.738
BM3D	2.234	5.072	2.283	4.165	1.369	4.640	0.177	0.948	2.341	2.326
NLM	1.535	6.511	1.701	4.498	−0.086	5.870	−4.236	0.472	1.630	1.495
SAIF	1.914	5.827	2.095	3.787	1.151	5.213	0.339	0.551	2.609	2.734
LPG-PCA	−0.601	5.501	0.217	2.945	−1.355	5.285	−1.547	−1.549	0.329	0.302
K-SVD	2.130	6.260	1.957	4.485	1.259	5.792	0.106	0.695	2.226	2.308
K-LLD	1.308	3.258	1.554	2.614	0.920	3.195	0.039	0.394	1.529	1.574

Table IV. FSIM results and FSIM improvements of denoising applied to images corrupted by ASCN ($\sigma_G = 1$) with $SD = 10$.

	TID2013 #1	TID2013 #3	TID2013 #5	TID2013 #7	TID2013 #13	TID2013 #23	Grass	USC-SIPI #7	FR Test #1	FR Test #2
Noisy AWGN	0.962	0.929	0.975	0.957	0.973	0.932	0.990	0.988	0.969	0.969
BM3D AWGN	0.011	0.046	0.009	0.027	0.001	0.049	0.001	0.002	0.011	0.012
Noisy	0.928	0.867	0.952	0.919	0.948	0.872	0.980	0.975	0.940	0.939
DCTF	0.027	0.077	0.012	0.039	0.011	0.076	0.001	0.002	0.022	0.021
BM3D	0.030	0.082	0.017	0.045	0.013	0.078	0.002	0.004	0.027	0.027
NLM	0.021	0.091	0.015	0.049	−0.006	0.093	−0.010	0.002	0.023	0.024
SAIF	0.030	0.092	0.017	0.048	0.013	0.088	0.003	0.003	0.029	0.031
LPG-PCA	−0.005	0.078	0.006	0.040	−0.029	0.091	−0.003	−0.007	0.013	0.016
K-SVD	0.031	0.094	0.015	0.049	0.012	0.093	0.001	0.003	0.027	0.027
K-LLD	0.020	0.059	0.012	0.030	0.010	0.057	0.001	0.002	0.018	0.018

by all techniques in an unsatisfactory manner. Practically there is no improvement due to denoising applied to the test image Grass. Moreover, NLM and LPG-PCA distort textures more than filtering out noise. Similar observations can be made for images TID2013 #13 and USC-SIPI #7 although improvements of PSNR are slightly better. For other images TID2013 #1, 5 and FR Test #1, 2 (we further call all of them as "miscellaneous"), analysis shows that moderate degree of noise spatial correlation influences not significantly (is not too different from AWGN case) on nonlocal approaches in cases of images with self-similarity content and homogeneous regions. Generally, we can say that there are a number of techniques able to handle moderate ASCN.

The corresponding results for MSSSIM are given in Table II. The values of MSSSIM for highly textural images (USC-SIPI #7 and Grass) that exceed 0.98 indicate that visual quality of noisy images is high due to masking effect of high-frequency components in textures [36]. On the contrary, test images with large-size homogeneous regions do not hide noise and, as the result, they have lower MSSSIM

values. Note that a small improvement of visual quality metric values shows that a considered filter is unable to suppress ASCN in high-frequency textures. This conclusion is in a good agreement with our previous research dealing with texture denoising under AWGN conditions [31–33]. For miscellaneous images with textures and rich-content regions, denoising efficiency is practically the same as for highly textured images. Thus, the recommendation for spatial correlation degree $\sigma_G = 0.8$ is to apply nonlocal denoising techniques only to simple-structure images.

For a larger spatial correlation degree $\sigma_G = 1$, the improvement of visual quality also depends upon image properties (see data for PSNR-HVS-M in Table III). The overall degradation of visual quality for this degree of ASCN with the same noise SD is notable for all images. It is obvious that for simple images the improvement of PSNR-HVS-M can be acceptable for BM3D, NLM, K-SVD and SAIF filters. Note that NLM efficiency assessed by PSNR-HVS-M shows the best results for simple images. This can be explained by the fact that low-frequency distortions are clearly perceived by the human visual system especially in homogeneous image

Table V. FSIM results of denoising applied to images corrupted by ASCN ($\sigma_G = 1.5$) with $SD = 15$.

	TID2013 #1	TID2013 #3	TID2013 #5	TID2013 #7	TID2013 #13	TID2013 #23	Grass	USC-SIPI #7	FR Test #1	FR Test #2
Noisy AWGN	0.929	0.869	0.953	0.919	0.949	0.873	0.981	0.976	0.941	0.941
BM3D AWGN	0.022	0.094	0.017	0.053	0.002	0.096	0.001	0.004	0.025	0.027
Noisy	0.827	0.702	0.880	0.807	0.869	0.709	0.945	0.927	0.854	0.852
DCTF	0.043	0.097	0.022	0.055	0.026	0.101	0.002	0.005	0.038	0.033
BM3D	0.050	0.102	0.031	0.062	0.031	0.100	0.004	0.010	0.046	0.042
NLM	0.070	0.192	0.043	0.104	0.037	0.189	−0.001	0.006	0.069	0.067
SAIF	0.059	0.155	0.035	0.082	0.035	0.152	0.006	0.005	0.064	0.061
LPG-PCA	0.071	0.183	0.039	0.098	0.040	0.180	0.004	0.011	0.064	0.061
K-SVD	0.076	0.194	0.042	0.106	0.040	0.197	0.004	0.010	0.070	0.068
K-LLD	0.033	0.076	0.023	0.046	0.023	0.078	0.003	0.004	0.034	0.031

Table VI. MSSSIM results of denoising applied to images corrupted by ASCN ($\sigma_G = 1.5$) with $SD = 15$.

	TID2013 #1	TID2013 #3	TID2013 #5	TID2013 #7	TID2013 #13	TID2013 #23	Grass	USC-SIPI #7	FR Test #1	FR Test #2
Noisy AWGN	0.925	0.826	0.952	0.905	0.936	0.845	0.987	0.966	0.942	0.937
BM3D AWGN	0.028	0.148	0.026	0.074	0.007	0.131	−0.000	0.011	0.032	0.038
Noisy	0.831	0.674	0.902	0.819	0.849	0.715	0.961	0.908	0.888	0.877
DCTF	0.030	0.115	0.021	0.061	0.016	0.107	−0.002	0.006	0.028	0.030
BM3D	0.035	0.119	0.027	0.067	0.020	0.108	−0.001	0.012	0.033	0.035
NLM	0.046	0.221	0.035	0.104	0.023	0.193	−0.014	0.006	0.047	0.054
SAIF	0.039	0.172	0.028	0.077	0.022	0.151	0.001	0.005	0.043	0.048
LPG-PCA	0.046	0.211	0.031	0.099	0.020	0.182	−0.004	0.009	0.042	0.048
K-SVD	0.053	0.216	0.035	0.104	0.027	0.194	−0.001	0.009	0.049	0.056
K-LLD	0.019	0.090	0.020	0.053	0.012	0.087	−0.001	0.004	0.026	0.027

regions. The kernel exploited in NLM smooths such notable distortions easily. Meanwhile, the textured images denoising by NLM have a negative effect. The reason is that the smoothing mechanism is not suited for irregular textures. LPG-PCA does not perform well due to the same reasons. The DCTF that has not been yet mentioned in our analysis demonstrates performance close to the general trend—high efficiency is achieved for simple-structure images and lack of improvement is observed for highly textured images. For miscellaneous images, one can see that K-SVD and SAIF in most cases have the highest efficiency compared to other techniques. Despite K-LLDs high performance of AWGN suppression, its performance is worse when compared to other filters for SCN.

In Table IV, FSIM metric results for moderate ASCN case are presented. FSIM values for noisy images and the corresponding improvements of simple-structure image denoising by nonlocal filters exploiting smoothing kernels for denoising point out that such filtering is expedient. Images from remote sensing FR Test #1, 2 are rich for small-sized features and textures. Denoising applied for

such images does not give notable improvement of visual quality and smears features of interest important for further processing or analysis. This relates to all considered filtering techniques.

An important conclusion is that $\sigma_G = 1$ can be treated as a borderline case when standard nonlocal denoising intended to suppress AWGN can be still applied for simple-structure and some miscellaneous images that contain self-similarity and are not highly textural. Expedience of image filtering for such images can be carried out automatically in a fast and accurate way [39].

Let us now present data for a large degree of SCN. Data for $\sigma_G = 1.5$ and $SD = 15$ are given below in Tables V and VI for visual quality metrics FSIM and MSSSIM. Comparing the corresponding data in Tables IV and V, it is seen that visual quality of noisy images significantly decreases if noise correlation and its intensity increase. Dependencies of noise suppression efficiency on image complexity are the same as earlier. The provided improvements are slightly larger than for $\sigma_G = 1$ and $SD = 10$. There are two reasons behind this. First, efficiency of noise suppression always improves if noise

Table VII. PSNR results of denoising applied to images corrupted by ASCN ($\sigma_G = 2$) with $SD = 15$.

	TID2013 #1	TID2013 #3	TID2013 #5	TID2013 #7	TID2013 #13	TID2013 #23	Grass	USC-SIPI #7	FR Test #1	FR Test #2
Noisy AWGN	24.627	24.626	24.652	24.626	24.646	24.635	24.749	24.643	24.698	24.653
BM3D AWGN	4.480	10.311	5.325	8.967	2.953	10.271	0.720	5.034	5.300	5.094
Noisy	24.608	24.607	24.634	24.608	24.620	24.617	24.731	24.617	24.686	24.625
DCTF	0.392	2.174	0.371	1.686	−0.257	2.238	−1.313	0.014	0.374	0.276
BM3D	0.716	2.485	0.946	2.129	−0.010	2.473	−1.011	0.577	0.951	0.806
NLM	1.037	4.942	1.379	3.526	−0.263	4.715	−3.586	0.487	1.372	1.147
SAIF	0.728	3.311	1.006	2.129	0.269	3.193	−0.602	0.125	1.338	1.253
LPG-PCA	0.502	4.227	0.562	2.829	−0.625	4.053	−2.296	0.318	0.601	0.390
K-SVD	0.935	4.618	1.048	3.200	0.174	4.592	−1.284	0.211	1.183	1.063
K-LLD	0.207	2.053	0.654	1.653	−0.186	2.209	−0.653	−0.095	0.598	0.535

SD increases. Second, FSIM metric has a nonlinear behavior. The results for the metric MSSSIM (see Table VI) are in good agreement with data in Table V. Simple-structure images are worth denoising while filtering highly textural images is still of question.

Finally, let us consider data for $\sigma_G = 2$. A part of data is presented in Tables VII and VIII. The following conclusions can be drawn. Although noise SD values are the same as considered earlier, it is obvious that the visual quality of test images corrupted by ASCN is decreased significantly according to PSNR-HVS-M. The filters NLM, K-SVD and LPG-PCA provide the best results for simple-structure and some miscellaneous images. At this time, the DCTF and BM3D filters do not perform well enough even for simple-structure images. This is because they do not take into account peculiarities of ASCN in the spectral domain. Practically for all texture and miscellaneous images there is no real gain of visual quality due to filtering. The visual quality metrics for noisy images are small and the improvement is small too. Some peculiarities of NLM should be stressed. It produces the best results for simple-structure and miscellaneous images and simultaneously produces sufficient distortions in highly textural images. LPG-PCA shows the results similar to NLM. K-LLD technique fails to perform well. The provided improvement of visual quality by the considered filters is sufficiently lower for large-degree ASCN than for AWGN case.

Summarizing the obtained results one can conclude the following. It is obvious that spatial correlation degree impacts negatively on visual quality of distorted images and denoising efficiency of all filters. Similar to AWGN case [31], filtering of textural images is the most problematic. Then any denoising can be canceled. For moderate ASCN, the nonlocal techniques SAIF, BM3D, K-SVD can perform appropriately. Spatial correlation degree $\sigma_G = 1$ is the borderline case in which filters adaptation to SCN can be neglected. In case of large degree of SCN the adaptation seems needed.

As we have seen, BM3D and DCTF can demonstrate appropriate performance for moderate degree of spatial
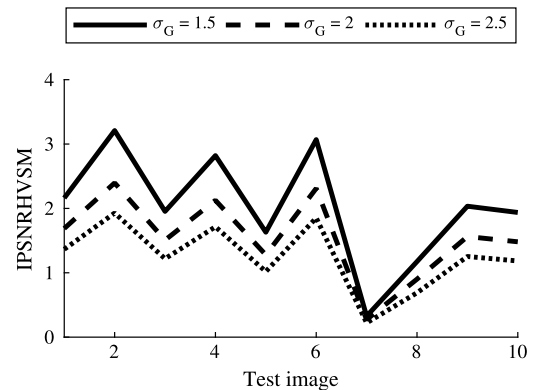
Figure 4. BM3D performance under large degree of SCN expressed by improvement of PSNR-HVS-M with noise $SD = 15$.

correlation of ASCN ($\sigma_G \leq 1$). Let us analyze BM3D performance for high degree of spatial correlation. In Figure 4, denoising efficiency is shown for ten test images and three degrees of spatial correlation. When spatial correlation degree becomes larger ($\sigma_G \geq 1$), improvement of PSNR-HVS-M decreases (Fig. 4). Thus we can confidently state that some adaptation of filters to noise characteristics is needed.

4. ASCN-ADAPTED DENOISING

As discussed in Section 2, SCN can be characterized by the normalized block spectrum. The SCN represented in spectral domain mostly occupies at low frequencies. This means that noise energy concentrates in such components. Local filters working in spectral domain are usually simple procedures due to linearity of applied transformations. DCTF uses the discrete cosine transform which is a simple procedure performed as block matrix multiplication. Direct and inverse transforms applied in blocks are:

$$B = T \cdot S \cdot T^T \tag{5}$$

$$S = T^T \cdot B \cdot T, \tag{6}$$

J. Imaging Sci. Technol.
IS&T International Symposium on Electronic Imaging 2019

060401-7

Nov.-Dec. 2018
Image Processing: Algorithms and Systems XVII

Table VIII. PSNR-HVS-M results of denoising applied to images corrupted by ASCN ($\sigma_G = 2$) with $SD = 15$.

	TID2013 #1	TID2013 #3	TID2013 #5	TID2013 #7	TID2013 #13	TID2013 #23	Grass	USC-SIPI #7	FR Test #1	FR Test #2
Noisy AWGN	27.927	26.983	28.516	27.583	28.178	27.096	31.019	29.089	28.345	28.362
BM3D AWGN	1.904	7.209	2.456	5.323	0.947	6.724	−0.303	0.788	2.324	2.487
Noisy	20.056	19.787	20.261	19.938	20.153	19.828	21.158	20.299	20.228	20.166
DCTF	1.249	2.104	0.951	1.691	0.933	2.073	0.094	0.446	1.088	1.048
BM3D	1.688	2.396	1.507	2.126	1.278	2.311	0.272	0.901	1.563	1.481
NLM	2.732	5.403	2.388	3.894	2.172	4.992	−0.248	0.986	2.622	2.547
SAIF	1.449	3.367	1.418	2.146	1.185	3.153	0.276	0.267	1.891	1.868
LPG-PCA	2.369	4.659	1.942	3.313	1.843	4.295	0.375	1.153	2.105	2.071
K-SVD	2.456	5.199	2.141	3.695	1.845	4.996	0.195	0.933	2.469	2.421
K-LLD	1.009	1.928	1.209	1.613	0.839	1.987	0.074	0.238	1.315	1.230

where S is a block in spatial domain, B is a transformed block (in 2D DCT domain), T is a transform matrix. Such transform implementation decreases computational burden and avoids iterative calculation of basis cosine functions for each block in the image. Its computation can be accelerated by parallel implementations on GPU or FPGA devices. Blocks with size 8x8 pixels are taken on the entire image with full overlapping [18]. The denoising by DCTF for each transformed block is performed by hard thresholding [27]:

$$B_{kl}^{\text{out}} = \begin{cases} B_{kl}^{\text{in}} \leftarrow \left| B_{kl}^{\text{in}} \right| > \beta \cdot \sigma \cdot W_{kl} \\ 0 \leftarrow \left| B_{kl}^{\text{in}} \right| \leq \beta \cdot \sigma \cdot W_{kl}, \end{cases} \quad (7)$$

where B^{in} is an input transformed block by Eq. (5), B^{out} is an output filtered block in transform domain, β is a thresholding parameter (the default value is 2.7), σ denotes the a priori known standard deviation of the ASCN that is assumed to be zero mean. The DCTF adaptation to noise spectrum consists of the following. The spectrum components that do not exceed the introduced frequency-dependent thresholds determined by noise standard deviation, β and normalized noise spectrum are assigned zero values. The DCT coefficient placed at k = 0 and l = 0 (DC component) that corresponds to mean level of a block is not used in filtering. After local block thresholding by Eq. (7), the inverse DCT is applied. To get a final filtered value for image pixel that can be covered by different partially overlapped blocks, the filtered values from all these blocks are averaged. Such mechanism essentially improves denoising efficiency compared to nonoverlapping DCTF version. The modified version of DCTF will be further called MDCTF.

In sense of used image data, the DCTF has a small computational cost and simple realization. BM3D filter works in the same manner as DCTF taking into account that denoising in a spectral domain is collaboratively applied to the group of identified similar blocks. Due to this, the first basic procedure (block matching) is essential for BM3D. The SCN presence makes the search for similar blocks more

complicated [40]. Thus, a similarity measure between blocks should be able to distinguish really similar blocks with respect to their content despite of ASCN presence. Hence, it is worth exploiting similarity measure that is robust to nonuniform normalized noise spectrum. It is useful to have such a measure because SCN correlation degree can vary depending on the nature of acquired images. According to the results given earlier [41] we propose to use the Canberra distance:

$$D_C = \sum_{k,l} \frac{|P_{kl} - B_{kl}|}{|P_{kl}| + |B_{kl}|}, \quad (8)$$

where B and P are the reference and candidate blocks in the transform domains for similarity search, D_C is a similarity measure value. This measure or distance is commonly used in cluster analysis [42] where data vectors contain disparate values of some object properties and is applied for grouping and hierarchy design. Despite to the real weights of different frequency components distorted by SCN, the Canberra measure summarizes relational impact of similarity among two corresponding values. This leads to practical robustness of this distance to the spatial correlation degree of SCN.

After similar blocks are found, the second basic procedure (namely, collaborative 3D filtering) is applied to the grouped blocks. Similar to the standard DCTF, the standard BM3D also uses a fixed (frequency-independent) threshold that in SCN case leads to reduction of filtering efficiency. Frequency-dependent thresholds for collaborative denoising are set in a similar manner as for MDCTF [41]. First, after all potentially similar blocks are transformed, similar blocks are grouped and represented in 3D combined transform domain. The separable 2D DCT transform and the 1D Haar transform in the similarity direction are applied and represented as a 2D array using column-vector presentation of each similar block. With respect to the size of obtained block groups, local denoising procedure creates a similar size 2D array where each column is the vectorized block of frequency-dependent thresholds used in Eq. (7) for MDCTF. The first row components that correspond to mean levels of

J. Imaging Sci. Technol.
IS&T International Symposium on Electronic Imaging 2019

060401-8

Nov.-Dec. 2018
Image Processing: Algorithms and Systems XVII
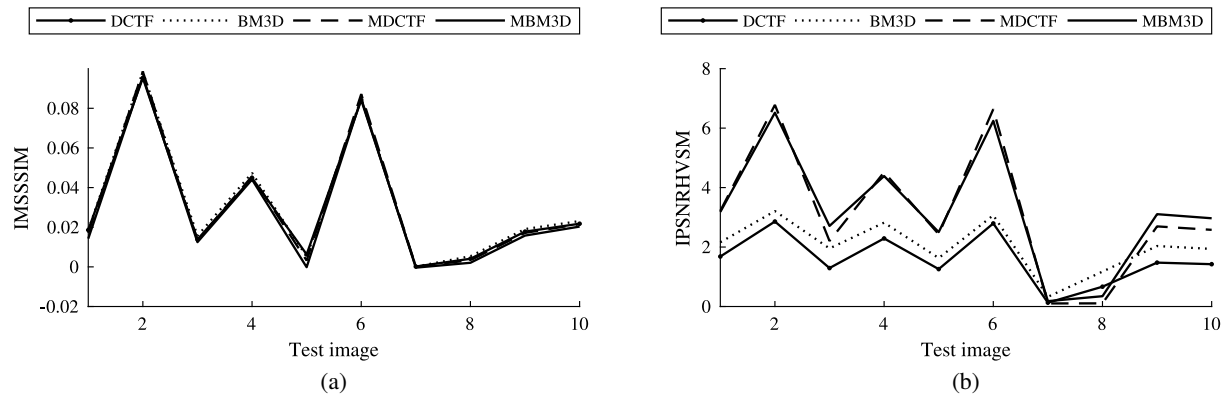
Figure 5. Denoising efficiency by improvements of (a) MSSSIM and (b) PSNR-HVS-M for (a) moderate ASCN ($\sigma_G = 0.8$, $SD = 10$) and (b) hard ASCN ($\sigma_G = 1.5$, $SD = 15$).

grouped blocks are not used. After collaborative filtering is performed, inverse 3D transform (first 1D Haar and then 2D DCT) have to be applied. The output filtered blocks are collected together like MDCTF in a cumulative manner and weighted with respect to the number of performed local operations with similar blocks. Thus, modifications of BM3D filter relate to block matching based on Canberra measure and adaptive thresholding.

5. COMPARATIVE ANALYSIS

For comparing the denoising efficiency of standard and modified versions of DCTF and BM3D, ten test images used in Section 2 are exploited in the same order. Figure 5 presents denoising results for two cases of ASCN—moderate $\sigma_G = 1$ (Fig. 5(a)) and large degree $\sigma_G = 1.5$ (Fig. 5(b)). For moderate case of ASCN it is apparent that performances of the adaptive versions MDCTF and MBM3D are close to the corresponding ones of standard filters. This confirms that moderate-degree SCN can be suppressed well without any modifications of the considered filters. On the contrary, to attenuate large degree of ASCN, the filter adaptation is required. The gain of both DCTF and MBM3D efficiency can reach up to 4 dB according to PSNR-HVS-M for simple-structure images and up to 2 dB even for textural images (for instance, TID2013 #13) and other miscellaneous images. For fully textural images like Grass or USC-SIPI #7 denoising is still useless.

Let us give examples of RS image fragment denoising by all considered filters including two adapted techniques. In Table IX, denoising examples of FR Test #1 image fragment under ASCN ($\sigma_G = 1.5$, $SD = 15$) are shown. In the noisy fragment, "grain"-like structure of ASCN and its high intensity can be observed. There are values of visual quality metrics for filtered entire images given under the corresponding image fragments. The DCTF output shows low-frequency residuals and smoothed small-sized features. There is no significant improvement for all metrics. LPG-PCA output slightly differs from DCTF—ASCN is suppressed better but all informative regions are more blurred. NLM copes with noise in the same manner

demonstrating better results than for LPG-PCA. The K-LLD technique attempts to preserve features in noisy data and shows results similar to DCTF. SAIF as an iterative version of NLM restores fine image details but has lower performance according to PSNR-HVS-M, FSIM and MSSSIM metrics due to worse noise suppression. Nonadapted BM3D cannot handle large-degree ASCN better than the aforementioned filters. The block matching procedure does not perform correctly. As a result, collaborative denoising is applied to distinct blocks. Besides, the fixed threshold does not allow removing ASCN components concentrated at low frequencies. K-SVD filter presents results comparable to SAIF and NLM suppressing the SCN with loss of fine details. The modified version of DCTF effectively attenuates the ASCN and preserves edges but introduces some artifacts near features of interest. The MBM3D with both modified block matching and 3D filtering demonstrates the best results for the considered example according to all metrics. The "grain"-structured noise is not practically visible and even small features are preserved without introducing any blur.

The full dataset and executable code that is used in experiments are available at https://github.com/asrubel/JIST 2019.

6. CONCLUSIONS

The presence of a spatially correlated noise impacts negatively the visual quality of acquired images. The real-life cases of SCN with different degrees of spatial correlation are analyzed in the spectral domain. The normalized noise block spectrum is proposed to characterize SCN which can be easily generated. Obtained denoising results for standard state-of-the-art techniques intended for AWGN suppression applied to SCN show that the use of such filters can be expedient only for a moderate degree of SCN and simple-structure images. The SCN cases with larger correlation degree cannot be handled by standard denoising techniques effectively. For this reason, the following modifications of 2D DCT-based filter and BM3D are proposed. First, frequency-dependent thresholds are set for both filters according to a normalized noise block spectrum. Second, Canberra distance robust

Table IX. Examples (extracted fragments of test image FR Test #1) of denoising by considered filters for hard ASCN case.

	Reference	Noisy	DCTF
PSNR	-	24.684	25.837
PSNR-HVS-M	-	21.266	22.742
FSIM	-	0.854	0.892
MSSIM	-	0.888	0.916
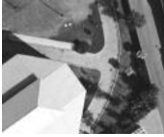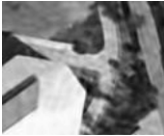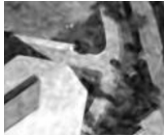
	LPG-PCA	NLM	K-LLD
PSNR	26.145	26.793	26.056
PSNR-HVS-M	23.93	24.297	22.761
FSIM	0.918	0.923	0.888
MSSIM	0.930	0.935	0.914

	SAIF	BM3D	K-SVD
PSNR	26.911	26.509	26.6
PSNR-HVS-M	23.68	23.3	24.099
FSIM	0.918	0.9	0.924
MSSIM	0.931	0.921	0.937

	MDCTF	MBM3D	
PSNR	27.303	27.703	
PSNR-HVS-M	23.961	24.372	
FSIM	0.918	0.927	
MSSIM	0.936	0.94	

with respect to noise spectrum is used in a block matching operation for BM3D. It is shown that the modified methods demonstrate better denoising efficiency than the standard filters even for large-degree SCN suppression.

REFERENCES

[1] W. K. Pratt, *Digital Image Processing*, 4th ed. (Wiley-Interscience, NY, 2007).

[2] A. Bovik, *Handbook of Image and Video Processing* (Academic Press, Cambridge, MA, 2000).

[3] C.-I. Chang, *Hyperspectral Data Exploitation: Theory and Applications* (Wiley-Interscience, NY, 2007).

[4] S. H. Lim, "Characterization of noise in digital photographs for image processing," Proc. SPIE **6069** (2006).

[5] X. Liu, S. Bourennane, and C. Fossati, "Nonwhite noise reduction in hyperspectral images," IEEE Geosci. Remote Sens. Lett. **9**, 368–372 (2012).

[6] B. W. Keelan, *Handbook of Image Quality* (Marcel Dekker Inc., New York, 2002).

[7] R. A. Touzi, "Review of speckle filtering in the context of estimation theory," IEEE Trans. Geosci. Remote Sens. **40**, 2392–2404 (2002).

[8] C. Oliver and S. Quegan, *Understanding Synthetic Aperture Radar Images* (SciTech Publishing, Raleigh, USA, 2004).

[9] R. A. Schowengerdt, *Remote Sensing: Models and Methods for Image Processing*, 3rd edn (Academic Press, Cambridge, MA, 2007).

[10] N. Ponomarenko, V. Lukin, K. Egiazarian, and L. Lepisto, "Adaptive visually lossless JPEG-based color image compression," Signal, Image and Video Processing **7**, 437–452 (2013).

[11] J. Aelterman, B. Goossens, A. Pizurica, and W. Philips, "Suppression of correlated noise," in *Recent Advances in Signal Processing*, edited by A. Zaher (IntechOpen, UK, 2009), pp. 211–236.

[12] P. Milanfar, "A tour of modern image filtering," IEEE Signal Process. Mag. **30**, 106–128 (2013).

[13] M. Lebrun, M. Colom, A. Buades, and J. M. Morel, "Secrets of image denoising cuisine," Acta Numerica **21**, 475–576 (2012).

[14] A. Buades, A. Coll, and J. M. Morel, "A non-local algorithm for image denoising," *Proc. 2005 IEEE Computer Vision and Pattern Recognition – CVPR'05* (IEEE, Piscataway, NJ, 2005), pp. 60–65.

[15] H. Talebi, X. Zhu, and P. Milanfar, "How to SAIF-ly boost denoising performance," IEEE Trans. Image Process. **22**, 1470–1485 (2013).

[16] L. Zhang, W. Dong, D. Zhang, and G. Shi, "Two-stage image denoising by principal component analysis with local pixel grouping," Pattern Recognit. **43**, 53–56 (2010).

[17] J. Portilla, V. Strela, M. J. Wainwright, and E. Simoncelli, "Image denoising using scale mixtures of gaussians in the wavelet domain," IEEE Trans. Image Process. **12**, 1338–1351 (2003).

[18] V. Lukin, R. Oktem, N. Ponomarenko, and K. Egiazarian, "Image filtering based on discrete cosine transform," Telecommun. Radio Eng. **66**, 1685–1701 (2007).

[19] K. Dabov, A. Foi, V. Katkovnik, and K Egiazarian, "Image denoising by sparse 3D transform-domain collaborative filtering," IEEE Transa. Image Process. **16**, 2080–2095 (2007).

[20] M. Aharon, M. Elad, and A. M. Bruckstein, "The K-SVD: An algorithm for designing of overcomplete dictionaries for sparse representations," IEEE Trans. Signal Process. **54**, 4311–4322 (2006).

[21] P. Chatterjee and P. Milanfar, "Clustering-based denoising with locally learned dictionaries," IEEE Trans. Image Process. **18**, 1438–1451 (2009).

[22] C.-A. Deledalle, F. Tupin, and L. Denis, "Patch similarity under non Gaussian noise," *Proc. IEEE Int'l. Conf. on Image Processing (ICIP)* (IEEE, Piscataway, NJ, 2011).

[23] M. Matrecano, G. Poggi, and L. Verdoliva, "Improved BM3D for correlated noise removal," *Proc. Int'l. Conf. on Computer Vision, Theory and Applications* (Springer, Rome, 2012), 1, pp. 129–134.

[24] B. Goossens, A. Pizurica, and W. Philips, "Removal of correlated noise by modeling the signal of interest in the wavelet domain," IEEE Trans. Image Process. **18**, 1153–1165 (2009).

[25] O. S. Rubel, V. V. Lukin, and F. S. de Medeiros, "Prediction of despeckling efficiency of DCT-based filters applied to SAR images," *Proc. Int'l. Conf. on Distributed Computing in Sensor Systems* (IEEE, Piscataway, NJ, 2015), pp. 159–168.

[26] M. Uss, V. Lukin, B. Vozel, and K. Chehdi, "Analysis of signal-dependent sensor noise on JPEG 2000-compressed Sentinel-2 multi-spectral images," Proc. SPIE **10427** (2017).

[27] N. Ponomarenko, V. Lukin, K. Egiazarian, and J. Astola, "A method for blind estimation of spatially correlated noise characteristics," Proc. SPIE **7532** (2010).

[28] N. Ponomarenko, O. Ieremeiev, V. Lukin, K. Egiazarian, L. Jin, J. Astola, B. Vozel, K. Chehdi, M. Carli, F. Battisti, and C.-C. Jay Kuo, "Color image database TID2013: peculiarities and preliminary results," *Proc. EUVIP* (IEEE, Piscataway, NJ, 2013), pp. 106–111.

[29] The USC-SIPI Image Database. Available http://sipi.usc.edu/database.

[30] V. Lukin, S. Abramov, A. Rubel, A. Naumenko, S. Krivenko, B. Vozel, K. Chehdi, K. Egiazarian, and J. Astola, "An approach to prediction of signal-dependent noise removal efficiency by DCT-based filter," Telecommun. Radio Eng. **73**, 1645–1659 (2014).

[31] A. Rubel, V. Lukin, M. Uss, B. Vozel, O. Pogrebnyak, and K. Egiazarian, "Efficiency of texture image enhancement by DCT-based filtering," Neurocomputing **155B**, 948–965 (2016).

[32] O. Rubel, V. Lukin, S. Abramov, B. Vozel, K. Egiazarian, and O. Pogrebnyak, "Efficiency of texture image filtering and its prediction," Signal Image and Video Process. **10**, 1543–1550 (2016).

33 O. Rubel, S. Abramov, V. Lukin, K. Egiazarian, B. Vozel, and A. Pogrebnyak, "Is texture denoising efficiency predictable?," Intl J. Pattern Recognit. Artif. Intell. **32**, 32 (2018).

34 P. Chatterjee and P. Milanfar, "Practical Bounds on Image Denoising: From estimation to information," IEEE Trans. Image Process. **20**, 1221–1233 (2011).

35 M. Uss, A. Rubel, V. Lukin, B. Vozel, and K. Chehdi, "Lower bound on image filtering mean squared error in the presence of spatially correlated noise," *Proc. on Microwaves, Radar and Remote Sensing Symposium – MRRS* (IEEE, Piscataway, NJ, 2014), pp. 10–13.

36 N. Ponomarenko, F. Silvestri, K. Egiazarian, M. Carli, J. Astola, and V. Lukin, "On between-coefficient contrast masking of DCT basis functions," *Proc. Int'l. Workshop on Video Processing and Quality Metrics VPQM-07* (Intel, Scottsdale, 2007).

37 L. Zhang, X. Mou, and D. Zhang, "FSIM: a feature similarity index for image quality assessment," IEEE Trans. Image Process. **20**, 2378–2386 (2011).

38 Z. Wang, E. Simoncelli, and A. Bovik, "Multiscale structural similarity for image quality assessment," *Conference Record of the Thirty-Seventh Asilomar Conf. on Signals, Systems and Computers* (IEEE, Piscataway, NJ, 2004), vol. 2, pp. 1398–1402.

39 O. Rubel, V. Lukin, and K. Egiazarian, "On prediction of DCT-based denoising efficiency under spatially correlated noise conditions," *Proc. TCSET'16* (IEEE, Piscataway, NJ, 2016), pp. 750–754.

40 A. S. Rubel, V. V. Lukin, and K. O. Egiazarian, "Metric performance in similar blocks search and their use in collaborative 3D filtering of grayscale images," Proc. SPIE **9019** (2014).

41 A. Rubel, V. Lukin, and K. Egiazarian, "Block matching and 3D collaborative filtering adapted to additive spatially correlated noise," *Proc. Ninth Int'l. Workshop on Video Processing and Quality Metrics for Consumer Electronics – VPQM'15* (Intel, Scottsdale, 2015).

42 S. Emran and N. Ye, "Robustness of Canberra metric in computer intrusion detection," *Proc. IEEE Workshop on Information Assurance and Security* (IEEE, Piscataway, NJ, 2001).